activation time sensitivity to hyperpolarization (*8*). The S2-S3 linker is also directed toward the S4/C-linker interface and may play a yet-unknown role in channel gating.

Summary

The structure of rEag1 reveals a non–domain swapped architecture of the S1 to S6 that is due to a short five-residue S4-S5 linker. This represents a divergence from the domain-swapped architecture of previous voltage-gated ion channel structures (Fig. 4) (*1*–*4*) and suggests a new paradigm for voltage-dependent gating for the Eag family of K_v channels. On the basis of the structure of Eag1, we propose a gating mechanism in which S4 enters the cytoplasm in a down or hyperpolarized state to interact with and induce a rotation of the C-linker and S6 in a direction that tightens the helical bundle to close the channel (Fig. 6B). In the up or depolarized state of the VS, S4 moves into the membrane, which allows the C-linker and S6 to rotate in a direction that loosens the helical bundle and thus relieves the high-energy bend in S6 to open the channel (Fig. 6B).

Two important consequences result from a gating mechanism in which the VS interacts with the cytoplasmic domains to gate the channel. First, this allows the cytoplasmic domains to close the channel independent of VS conformation. This is observed in the structure of Eag1, as binding of CaM to the cytoplasmic domains closes the pore, but the VS is in the up or depolarized conformation. Second, this provides an added level of regulation through the interaction of intracellular domains with the voltage-dependent gating machinery. In Eag1, the N terminus of the PAS domain, which confers sensitivity to hyperpolarization (*8*), is poised to interact with the S4 and S4-S5 linker in a closed conformation (Fig. 5D).

REFERENCES AND NOTES

1. S. B. Long, E. B. Campbell, R. Mackinnon, *Science* **309**, 897–903 (2005).
2. S. B. Long, X. Tao, E. B. Campbell, R. MacKinnon, *Nature* **450**, 376–382 (2007).
3. J. Payandeh, T. Scheuer, N. Zheng, W. A. Catterall, *Nature* **475**, 353–358 (2011).
4. J. Wu *et al*., *Science* **350**, aad2395 (2015).
5. S. B. Long, E. B. Campbell, R. Mackinnon, *Science* **309**, 903–908 (2005).
6. H. R. Guy, S. R. Durell, J. Warmke, R. Drysdale, B. Ganetzky, *Science* **254**, 730 (1991).
7. M. Ju, D. Wray, *Biochem. Biophys. Res. Commun.* **342**, 1088–1097 (2006).
8. H. Terlau, S. H. Heinemann, W. Stühmer, O. Pongs, J. Ludwig, *J. Physiol.* **502**, 537–543 (1997).
9. J. H. Morais Cabral *et al*., *Cell* **95**, 649–655 (1998).
10. F. W. Muskett *et al*., *J. Biol. Chem.* **286**, 6184–6191 (2011).
11. J. Wang, M. C. Trudeau, A. M. Zappia, G. A. Robertson, *J. Gen. Physiol.* **112**, 637–647 (1998).
12. W. N. Zagotta *et al*., *Nature* **425**, 200–205 (2003).
13. T. I. Brelidze, A. E. Carlson, W. N. Zagotta, *J. Biol. Chem.* **284**, 27989–27997 (2009).
14. T. I. Brelidze, A. E. Carlson, B. Sankaran, W. N. Zagotta, *Nature* **481**, 530–533 (2012).
15. M. J. Marques-Carvalho *et al*., *J. Mol. Biol.* **423**, 34–46 (2012).
16. Y. Haitin, A. E. Carlson, W. N. Zagotta, *Nature* **501**, 444–448 (2013).
17. J. Ludwig *et al*., *EMBO J.* **13**, 4451–4458 (1994).
18. R. Schönherr, K. Löber, S. H. Heinemann, *EMBO J.* **19**, 3263–3271 (2000).
19. U. Ziechner *et al*., *FEBS J.* **273**, 1074–1086 (2006).
20. L. S. Mortensen *et al*., *J. Physiol.* **593**, 181–196 (2014).
21. P. Bijlenga *et al*., *J. Physiol.* **512**, 317–323 (1998).
22. L. A. Pardo, A. Brüggemann, J. Camacho, W. Stühmer, *J. Cell Biol.* **143**, 767–775 (1998).
23. L. A. Pardo *et al*., *EMBO J.* **18**, 5540–5547 (1999).
24. B. Hemmerlein *et al*., *Mol. Cancer* **5**, 41 (2006).
25. J. R. Agarwal, F. Griesinger, W. Stühmer, L. A. Pardo, *Mol. Cancer* **9**, 18 (2010).
26. F. Mello de Queiroz, G. Suarez-Kurtz, W. Stühmer, L. A. Pardo, *Mol. Cancer* **5**, 42 (2006).
27. B. R. Downie *et al*., *J. Biol. Chem.* **283**, 36234–36240 (2008).
28. D. Gómez-Varela *et al*., *Cancer Res.* **67**, 7343–7349 (2007).
29. J. García-Quiroz *et al*., *PLOS ONE* **7**, e45063 (2012).
30. J. Ludwig, D. Owen, O. Pongs, *EMBO J.* **16**, 6337–6345 (1997).
31. M. Ju, D. Wray, *FEBS Lett.* **524**, 204–210 (2002).
32. Y. Jiang *et al*., *Nature* **423**, 33–41 (2003).
33. Single-letter abbreviations for the amino acid residues are as follows: A, Ala; C, Cys; D, Asp; E, Glu; F, Phe; G, Gly; H, His; I, Ile; K, Lys; L, Leu; M, Met; N, Asn; P, Pro; Q, Gln; R, Arg; S, Ser; T, Thr; V, Val; W, Trp; and Y, Tyr.
34. P. H. Hsu *et al*., *PLOS ONE* **7**, e41203 (2012).
35. X. Tao, A. Lee, W. Limapichat, D. A. Dougherty, R. MacKinnon, *Science* **328**, 67–73 (2010).
36. M. Zhang, J. Liu, G. N. Tseng, *J. Gen. Physiol.* **124**, 703–718 (2004).
37. S. K. Aggarwal, R. MacKinnon, *Neuron* **16**, 1169–1177 (1996).
38. S. A. Seoh, D. Sigg, D. M. Papazian, F. Bezanilla, *Neuron* **16**, 1159–1167 (1996).
39. Z. Lu, A. M. Klem, Y. Ramu, *Nature* **413**, 809–813 (2001).
40. D. del Camino, M. Holmgren, Y. Liu, G. Yellen, *Nature* **403**, 321–325 (2000).
41. É. Lörinczi *et al*., *Nat Commun* **6**, 6672 (2015).
42. R. M. Hardman, P. J. Stansfeld, S. Dalibalta, M. J. Sutcliffe, J. S. Mitcheson, *J. Biol. Chem.* **282**, 31972–31981 (2007).
43. G. Barbato, M. Ikura, L. E. Kay, R. W. Pastor, A. Bax, *Biochemistry* **31**, 5269–5278 (1992).

ACKNOWLEDGMENTS

We thank M. Ebrahim at the Rockefeller University cryo-EM resource center for help with data collection and J. Chen and members of the MacKinnon laboratory for helpful discussions. This work was supported in part by NIH grant GM43949. J.R.W. is a Damon Runyon Fellow supported by the Damon Runyon Cancer Research Foundation (DRG-2212-15) and R.M. is an investigator in the Howard Hughes Medical Institute. The low-pass filtered and amplitude-modified three-dimensional cryo-EM density maps for rEag1 have been deposited in the EM Data Bank with accession code EMD-8215. Atomic coordinates for rEag1 have been deposited in the Protein Data Bank under accession code 5K7L. J.R.W. performed functional experiments and expressed, purified, and determined single-particle cryo-EM structure of rEag1. J.R.W. and R.M. designed experiments, analyzed and interpreted results, and wrote the manuscript.

SUPPLEMENTARY MATERIALS

www.sciencemag.org/content/353/6300/664/suppl/DC1
Materials and Methods
Figs. S1 to S9
References (*44*–*65*)

1 April 2016; accepted 22 June 2016
10.1126/science.aaf8070

PHYSICS

Laser spectroscopy of muonic deuterium

Randolf Pohl,[1,2]* François Nez,[3] Luis M. P. Fernandes,[4] Fernando D. Amaro,[4] François Biraben,[3] João M. R. Cardoso,[4] Daniel S. Covita,[5] Andreas Dax,[6] Satish Dhawan,[6] Marc Diepold,[1] Adolf Giesen,[7,8]† Andrea L. Gouvea,[4] Thomas Graf,[7] Theodor W. Hänsch,[1,9] Paul Indelicato,[3] Lucile Julien,[3] Paul Knowles,[10]‡ Franz Kottmann,[11] Eric-Olivier Le Bigot,[3] Yi-Wei Liu,[12] José A. M. Lopes,[4,13] Livia Ludhova,[10]§ Cristina M. B. Monteiro,[4] Françoise Mulhauser,[10,1]|| Tobias Nebel,[1]¶ Paul Rabinowitz,[14] Joaquim M. F. dos Santos,[4] Lukas A. Schaller,[10] Karsten Schuhmann,[11,8,15] Catherine Schwob,[3] David Taqqu,[15] João F. C. A. Veloso,[5] Aldo Antognini,[1,11,15] The CREMA Collaboration

The deuteron is the simplest compound nucleus, composed of one proton and one neutron. Deuteron properties such as the root-mean-square charge radius r_d and the polarizability serve as important benchmarks for understanding the nuclear forces and structure. Muonic deuterium μd is the exotic atom formed by a deuteron and a negative muon μ^-. We measured three 2S-2P transitions in μd and obtain r_d = 2.12562(78) fm, which is 2.7 times more accurate but 7.5σ smaller than the CODATA-2010 value r_d = 2.1424(21) fm. The μd value is also 3.5σ smaller than the r_d value from electronic deuterium spectroscopy. The smaller r_d, when combined with the electronic isotope shift, yields a "small" proton radius r_p, similar to the one from muonic hydrogen, amplifying the proton radius puzzle.

Precision spectroscopy of atomic energy levels can be used to determine properties of the nucleus (*1*). Deuterium (D), for example, is a heavier isotope of hydrogen (H), with a nucleus, the deuteron (d), composed of one proton and one neutron (*2*). D was discovered through a tiny shift in the Balmer spectral lines of D-enriched hydrogen (*3*). This shift is caused mainly by the mass difference between the proton and the deuteron. Today, the nuclear masses are accurately known from cyclotron frequency measurements in a Penning trap

(*1*), and the measured isotope shift of the 1S-2S transition in H and D (*4*) determines the (squared) deuteron-proton charge radius difference (*5*)

$$\delta^{(2)}(\mathrm{H,D}) \equiv r_\mathrm{d}^2 - r_\mathrm{p}^2 = 3.82007(65)\ \mathrm{fm}^2 \quad (1)$$

This is because the wave function of atomic S states is maximal at the origin, where the nucleus resides, and the wave function overlap with the extended nuclear charge distribution reduces the atomic binding energy. Equation 1 links measurements of transition frequencies in H and D. These, together with elastic electron scattering on protons (*6*) and deuterons (*7*), determine the Rydberg constant R_∞, r_p and r_d in the CODATA adjustment of the fundamental physical constants (*1*).

Muonic atoms are a special class of "exotic" atoms that offer access to nuclear properties with much higher accuracy. In a muonic atom, the nucleus is orbited by one negative muon μ^-, instead of the usual electrons e^-. The muon's larger mass $m_\mu = 207 m_e$ results in a muonic Bohr radius that is smaller than the corresponding electronic Bohr radius by the ratio of reduced masses $m_\mathrm{red} = m_\ell m_\mathrm{nuc}/(m_\ell + m_\mathrm{nuc})$. Here m_ℓ is the mass of the lepton (muon μ^- or electron e^-), and m_nuc is the mass of the nucleus. As the Bohr radius shrinks proportionally to $1/m_\mathrm{red}$, the overlap of the muon's wave function with the nuclear charge distribution increases as m_red^3. For μd, $m_\mathrm{red} = 196 m_e$, and the wave function overlap is $(m_\mathrm{red}/m_e)^3 \approx 10^7$ larger in μd than in D. A measurement of the Lamb shift (2P-2S energy difference) in μd is therefore extremely sensitive to the deuteron charge radius r_d.

Our recent measurements of the Lamb shift in muonic hydrogen μp have resulted in a value of the proton charge radius r_p = 0.84087(39) fm, which is 10 times more accurate, but 4%, or 7σ, smaller (*8*, *9*) than the CODATA-2010 value (*1*), which is the most recently published CODATA compilation. This so-called "proton radius puzzle" has questioned the correctness of various experiments or quantum electrodynamics (QED) calculations, the value of the Rydberg constant, our understanding of the proton structure, or the standard model of particle physics (*10*, *11*).

Here we present measurements of the three 2S-2P transitions in μd highlighted in Fig. 1, yielding a precise value of r_d. The principle of the experiment is to form μd atoms in the metastable 2S state (*12*) and to measure the 2S-2P transitions by pulsed laser spectroscopy. Comparison with theory (*13*) reveals r_d. The muonic deuterium data presented here were acquired in the same measurement period as the muonic hydrogen data in (*8*, *9*). Independent and reliable calculations of QED (*14*–*17*) and nuclear structure effects (*18*–*22*) in μd, which are required to interpret the experiment, have recently become available and are summarized in (*13*).

Measurement of the spectral lines of muonic deuterium

The experiment has been described before (*8*, *9*). In brief, a 5 × 12 mm^2 beam of low-energy negative muons μ^- (3-keV kinetic energy, average rate 600/s) is stopped in a 20-cm-long target filled with 1 hPa of D_2 gas at 20°C. A pulsed laser system (*23*, *24*) is triggered on the detection of a single arriving muon and provides pulses with an energy of ~0.25 mJ, tunable around a wavelength of 6 μm, and calibrated against water vapor absorption lines known within a few megahertz (*25*). A multipass mirror cavity (*26*) ensures good laser illumination of the muon stop volume. Large-area avalanche photo diodes (*27*, *28*) detect the 2-keV K_α x-rays from the radiative 2P→1S transition that follows the laser-induced 2S→2P excitation of μd. The laser frequency is changed every few hours, and the resonances displayed in Fig. 2 are obtained by plotting the number of 2-keV x-rays (normalized to the number of stopped muons) detected in time coincidence with the laser pulse, as a function of laser frequency. On the peak of the resonance, we recorded up to 10 laser-induced x-rays ("events") per hour with all data reduction cuts (*9*) applied. The background level of about 2 events per hour originates mainly from misidentified muon decay electrons. About a third of the recorded events are without laser light, providing the expected background level shown as horizontal bands in Fig. 2. The resonances are fitted with a flat background plus a Lorentzian line shape model that takes into account varying laser pulse energies and saturation effects.

The three resonances shown in Fig. 2 are the μd transitions $2S_{1/2}^{F=3/2} \rightarrow 2P_{3/2}^{F=5/2}$, $2S_{1/2}^{F=1/2} \rightarrow 2P_{3/2}^{F=3/2}$, and $2S_{1/2}^{F=1/2} \rightarrow 2P_{3/2}^{F=1/2}$, abbreviated as #1, #2, and #3, respectively. Their positions and uncertainties are

$$\nu_1 = 50816.27 \pm 0.84(\mathrm{stat}) \pm 0.35(\mathrm{syst})\ \mathrm{GHz} \quad (2)$$

$$\nu_2 = 52061.2 \pm 2.0(\mathrm{stat}) \pm 0.35(\mathrm{syst})\ \mathrm{GHz} \quad (3)$$

$$\nu_3 = 52154.1 \pm 2.2(\mathrm{stat}) \pm 0.35(\mathrm{syst})\ \mathrm{GHz} \quad (4)$$

The systematic uncertainties of 0.35 GHz arise from laser frequency fluctuations (*8*) and Zeeman shifts from a conceivable small admixture of circular polarized light and the 5 T magnetic field of the muon beam line. Line-pulling effects from off-resonant excitation of neighboring levels are negligible (*29*).

Deuteron charge radius

For the fit of line #1, the Lorentzian width was fixed to the natural radiative line width of Γ = 19.5 GHz (*8*, *9*), as the freely fitted value Γ = 13.1 GHz is 2.6σ too small. Both fits agreed on the line center within 0.33 GHz, and the uncertainty quoted in Eq. 2 is the larger one from the fit with fixed width. The difference $\nu_3 - \nu_2$ = 92.9 ± 3.0 GHz from the fit is in good agreement (1.5σ) with the theoretical value of 88.045 GHz (*13*). The amplitude of line #3 is larger than zero only with a significance of 4.5σ, but it serves to identify line #2 unambiguously. The alternative—namely, that the left peak in Fig. 2 (bottom) is in fact line #3—is disfavored with 6.9σ significance thanks to the absence of a peak with twice the amplitude ~90 GHz left of line #2.

Combining the three measured frequencies and using the theoretical 2P fine structure and $2P_{3/2}$ hyperfine splittings (*13*), we determine the 2P-2S Lamb shift (LS) and 2S hyperfine splitting (HFS) in μd

$$\Delta E_\mathrm{LS}^\mathrm{exp} = 202.8785(31)_\mathrm{stat}(14)_\mathrm{syst}\ \mathrm{meV} \quad (5)$$

$$\Delta E_\mathrm{HFS}^\mathrm{exp} = 6.2747(70)_\mathrm{stat}(20)_\mathrm{syst}\ \mathrm{meV} \quad (6)$$

with total experimental uncertainties of 0.0034 and 0.0073 meV, respectively. The measured 2S

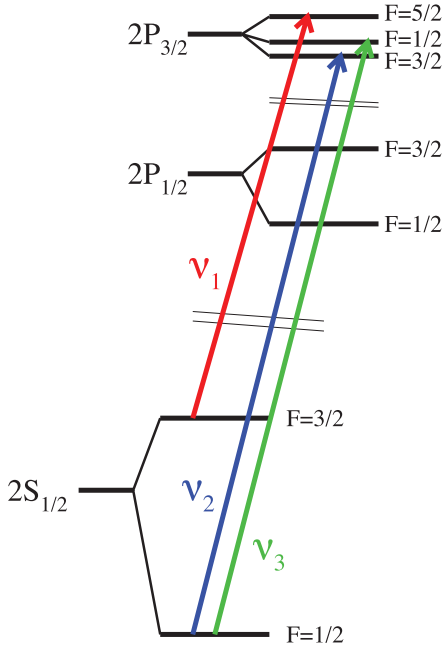

Fig. 1. *n* = 2 levels in muonic deuterium. The order of the $2P_{3/2}$ sublevels is changed by the nuclear quadrupole moment (*13*). The three measured transitions are indicated.

[1]Max-Planck-Institut für Quantenoptik, 85748 Garching, Germany. [2]Johannes Gutenberg-Universität Mainz, QUANTUM, Institut für Physik & Exzellenzcluster PRISMA, 55099 Mainz, Germany. [3]Laboratoire Kastler Brossel, UPMC-Sorbonne Universités, CNRS, Ecole Normale Supérieure–PSL Research University, Collège de France, 75005 Paris, France. [4]LIBPhys, Department of Physics, University of Coimbra, 3004-516 Coimbra, Portugal. [5]I3N, Departamento de Física, Universidade de Aveiro, 3810-193 Aveiro, Portugal. [6]Physics Department, Yale University, New Haven, CT 06520-8121, USA. [7]Institut für Strahlwerkzeuge, Universität Stuttgart, 70569 Stuttgart, Germany. [8]Dausinger + Giesen GmbH, Rotebühlstrasse 87, 70178 Stuttgart, Germany. [9]Ludwig-Maximilians-Universität, Munich, Germany. [10]Département de Physique, Université de Fribourg, 1700 Fribourg, Switzerland. [11]Institute for Particle Physics, ETH Zurich, 8093 Zurich, Switzerland. [12]Physics Department, National Tsing Hua University, Hsinchu 300, Taiwan. [13]Instituto Politécnico de Coimbra, ISEC, 3030–199, Portugal. [14]Department of Chemistry, Princeton University, Princeton, NJ 08544-1009, USA. [15]Paul Scherrer Institute, 5232 Villigen–PSI, Switzerland.

***Corresponding author. Email: pohl@uni-mainz.de** †Present address: Deutsches Zentrum für Luft- und Raumfahrt e.V. in der Helmholtz-Gemeinschaft, 70569 Stuttgart, Germany. ‡Present address: LogrusData, Vienna, Austria. §Present address: Forschungszentrum Jülich IKP-2 and RWTH Aachen University, Germany. ||Present address: International Atomic Energy Agency, Vienna, Austria. ¶Present address: Honeywell Process Solutions Inc, 500 Brooksbank Avenue, North Vancouver BC V7J 3S4, Canada.

HFS is in excellent agreement with the theoretical value, $\Delta E_{\mathrm{HFS}}^{\mathrm{theo}} = 6.2791(50)$ meV (*13*).

The Lamb shift in μd is extraordinarily sensitive (*13*) to the root mean square (RMS) deuteron charge radius

$$\Delta E_{\mathrm{LS}}^{\mathrm{theo}} = 228.7766(10)\ \mathrm{meV} + \Delta E_{\mathrm{LS}}^{\mathrm{TPE}} \qquad (7)$$

$$-6.1103(3)\, r_{\mathrm{d}}^2\ \mathrm{meV/fm^2}$$

where

$$\Delta E_{\mathrm{LS}}^{\mathrm{TPE}}(\mathrm{theo}) = 1.7096(200)\ \mathrm{meV} \qquad (8)$$

is the deuteron polarizability contribution (*13*) from two-photon exchange (TPE), recently calculated with good accuracy (*18*–*22*). The charge radius effect in Eq. 7 contributes as much as 14% to the 2P-2S Lamb shift, which explains the excellent sensitivity of our measurement to r_{d}. We obtain r_{d} from equating Eqs. 5 and 7, and using Eq. 8, which yields

$$r_{\mathrm{d}}(\mu\mathrm{d}) = 2.12562(13)_{\mathrm{exp}}(77)_{\mathrm{theo}}\ \mathrm{fm} \qquad (9)$$

where the theory uncertainty is almost exclusively from $\Delta E_{\mathrm{LS}}^{\mathrm{TPE}}$ (Eq. 8). This radius is in 7.5σ disagreement with the CODATA value (*1*), which is the best estimate of the deuteron radius obtained from precision spectroscopy of H and D and electron scattering on protons and deuterons,

$$r_{\mathrm{d}}(\mathrm{CODATA}) = 2.1424(21)\ \mathrm{fm} \qquad (10)$$

(see Fig. 3). We are hence faced with the fact that precision determinations of the Lamb shift in both μp and μd, from a total of five measured resonances, each show a ≥7σ discrepancy to the predictions based on fundamental physical constants from the self-consistent CODATA world average (*1*), carefully checked QED calculations (*13*, *30*), and physics within the standard model.

The CODATA deuteron radius r_{d} is tightly linked to the CODATA proton radius r_{p}, by virtue of Eq. 1. However, as detailed in (*31*), we have deduced a deuteron charge radius considering spectroscopy data in regular deuterium alone—i.e., without relying on the value of the proton radius. This yields a value of

$$r_{\mathrm{d}}(\mathrm{D\ spectroscopy}) = 2.1415(45)\ \mathrm{fm} \qquad (11)$$

in excellent agreement with the CODATA value, but 3.5σ larger than the value obtained here from muonic deuterium (see Fig. 3, blue point, "D spectroscopy").

This distinct 3.5σ discrepancy between the atomic physics determinations of r_{d} from D and μd is almost as severe as the 4.0σ atomic physics discrepancy between the r_{p} values from H spectroscopy [see (*1*), table XXXVIII, adjustment 8] and μp (*9*) (see Fig. 4). These two discrepancies are independent, as explained in (*31*).

The difference between the deuteron radii from the spectroscopy of electronic and muonic deuterium is only 0.017 fm, or 0.8%. Thus, even though the deuteron charge radius $r_{\mathrm{d}}(\mathrm{e\text{–}d\ scatt.}) = 2.130(10)$ fm, extracted from elastic electron-deuteron scattering (*7*), is accurate to 0.5%, it is unfortunately not accurate enough to distinguish between the values from μd and CODATA.

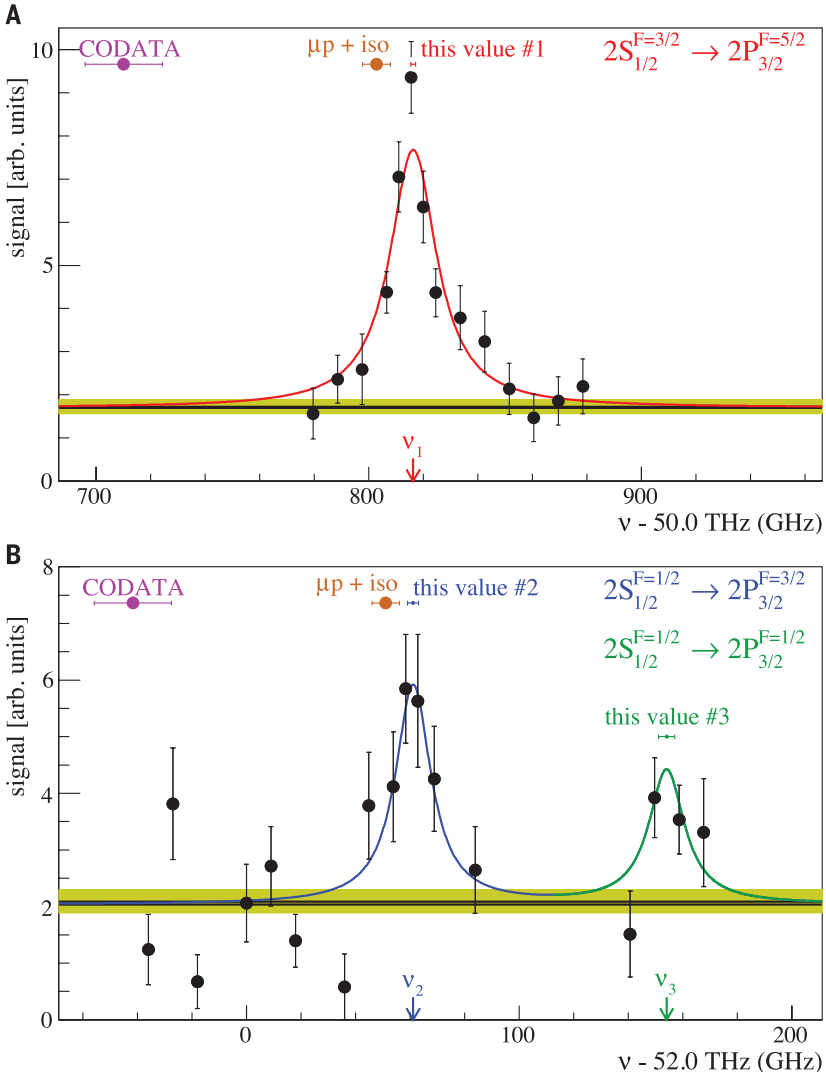

Fig. 2. Three measured resonances in muonic deuterium. The resonances are labeled #1 (**A**), and #2 and #3 (**B**). The signal (*y* axis) is "normalized number of events" as described in (*8*). Predicted resonance positions are shown based on Eqs. 7 and 8: The CODATA-2010 deuteron radius (pink, Eq. 10) would correspond to ~104 GHz lower resonance positions, which is a difference of 7.5σ. The "expected" deuteron radius Eq. 13, ("μp + iso," brown) obtained by combining the proton radius from muonic hydrogen (*9*) and the electronic isotope shift ("iso"), Eq. 1, is consistent with the observed resonance positions within ~2.6σ. The top and bottom panel's data were recorded in 1 week and 2 days, respectively. As an example, the three highest points around the peak of resonance #1 contain a total of 260 events, recorded in 21 hours.

Proton and deuteron radius puzzle

Many attempts to explain the proton radius discrepancy exist (*10*, *11*). Our muonic deuterium result provides fresh insight, as the so-called "proton radius puzzle" is in fact not limited to the proton; there is a distinct deuteron radius puzzle. Using r_{d} (CODATA) in Eq. 7 yields a Lamb shift that is $\varepsilon_{LS}(\mu\mathrm{d}) = 0.438(59)$ meV smaller than the measured value, Eq. 5, and hence resonance frequencies that are ~104 GHz smaller than observed (Fig. 2). The $\varepsilon_{LS}(\mu\mathrm{d})$ is even somewhat larger than the proton radius discrepancy $\varepsilon_{LS}(\mu\mathrm{p}) = 0.329(47)$ meV between the LS we observed in μp and the one calculated with the CODATA value of r_{p} (*9*).

The ratio of discrepancies in μd and μp, $\varepsilon_{LS}(\mu\mathrm{d})/\varepsilon_{LS}(\mu\mathrm{p}) = 1.3(2)$ is in agreement with the ratio of the wave-function overlap from the reduced mass ratio, $[m_{\mathrm{red}}(\mu\mathrm{d})/m_{\mathrm{red}}(\mu\mathrm{p})]^3 = 1.17$. Such a scaling is expected for several beyond–standard model (BSM) physics scenarios (*10*, *11*, *32*–*34*), where a new force between muons and protons is

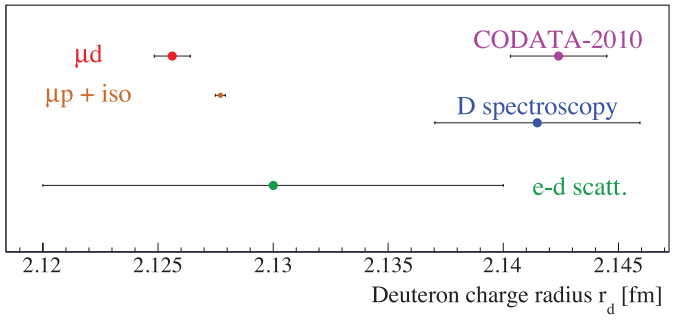

Fig. 3. Deuteron radii. Our value Eq. 9 ("μd," red) has a 7.5σ discrepancy with the CODATA-2010 value (*1*), but is within 2.6σ of the smaller "expected" value Eq. 13 ("μp + iso," brown, see text), obtained by combining the proton radius from muonic hydrogen (*9*) and the electronic isotope shift, Eq. 1. The value from laser spectroscopy of electronic deuterium ("D spectroscopy," blue, Eq. 11) is obtained as detailed in (*31*) and is 3.5σ larger than the μd value. The world average from elastic e-d scattering (*7*) ("e-d scatt," green) is also shown.

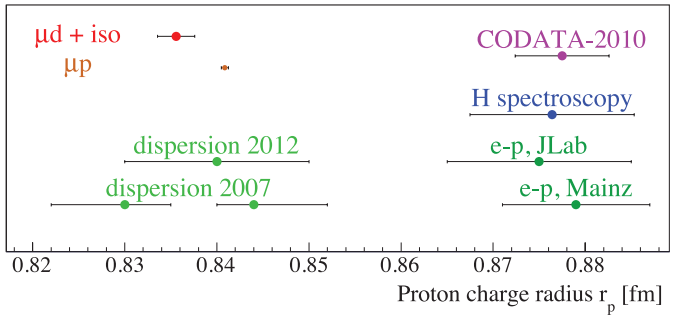

Fig. 4. Proton radii. Shown are the values deduced from muonic hydrogen (*9*) ("μp," brown) and from muonic deuterium (Eq. 9, "μd + iso," red), which both differ by >7σ from the CODATA-2010 value (*1*). Many other determinations exist, and we highlight the values from spectroscopy of H (but not D), from CODATA-2010 [(*1*), table XXXVIII, adjustment 8] ("H spectroscopy", blue); elastic electron-proton scattering (dark green) from (*6*) and (*47*); and electron scattering data analyses based on dispersion relations (light green), both less recent (*48*) and more recent (*49*) than the μp value (*8*, *9*). Many more values exist (*50*).

responsible for the change in the observed LS and can at the same time explain the long-standing ~ 3.5σ discrepancy in the muon g-2 value (*35*). In these models, the coupling of such a new force to neutrons must be negligible to fulfill other experimental constraints. The same scaling is also expected for explanations based on an unexpectedly large TPE contribution to proton polarizability (*36*), or an effect of a "sea of leptons" inside the proton (*37*, *38*).

Before resorting to BSM solutions, however, one should investigate what it would take to "solve" the two discrepancies within SM physics. As noted before (*8*–*11*), and explained in more detail in (*31*), the reconciliation of electronic and muonic spectroscopy data still requires rather drastic measures.

For one, the CODATA Rydberg constant could be wrong by ~ 7σ—for example, because of a yet-undiscovered, common systematic effect in the most precise measurements of transitions from the 2S to the 8S, 8D, and 12D states in H and D (*39*). Such a change of R_∞ would shift the proton radius from H to the smaller μp value (*8*–*10*, *31*). It would also bring the deuteron radius from D to within ~ 2.5σ of the μd value (see below).

Alternatively, the QED theory of the Lamb shift in electronic H and D could be missing a large contribution of ~110 kHz, which corresponds to about 44 times the claimed theory uncertainty (44σ) of ~2.5 kHz. Such a missing QED contribution would bring the charge radii from H and D spectroscopy into agreement with their muonic counterparts, without changing the Rydberg constant (*31*).

Third, a systematic shift of all spectroscopic muonic measurements by 140σ (corresponding to 80 GHz in μp and 104 GHz in μd), or a missing theory term in the Lamb shift of muonic atoms that accounts for the missing ε_{LS}, could be the source of the discrepancies. This theory error would correspond to 160σ in μp, and 22σ in μd, where the uncertainty of the TPE contribution is about 10 times larger (*13*). The claimed uncertainty of the pure QED (i.e., non-TPE) contributions in μd (μp) is about 440 (220) times smaller than the ε_{LS} (*13*).

Neither a shift of R_∞ by 7σ from the CODATA value, nor a change of the LS in H and D by ~ 110 kHz, will, however, appreciably affect Eq. 1 (*5*). Hence, we can proceed and draw conclusions from the fact that the muonic isotope shift

$$\delta^{(2)}(\mu p, \mu d) = 3.81120(339)\ \text{fm}^2 \qquad (12)$$

is compatible within 2.6σ with the "electronic" isotope shift, Eq. 1, but five times less accurate. The absolute values of r_p and r_d from the muonic 2S-2P measurements are thus roughly consistent with the size difference from the electronic 1S-2S measurement (*4*, *5*), Eq. 1.

The dominant source of uncertainty in Eq. 12 is the calculated TPE contribution (Eq. 8), whose effect on the uncertainty of r_d from μd, Eq. 9, is about six times larger than the experimental uncertainty. Hence, we are tempted to ascribe the remaining 2.6σ discrepancy between the electronic and muonic isotope shift to the TPE contribution to the LS in μd.

We can thus use the muonic proton radius from μp (*9*), $r_p(\mu p) = 0.84087(39)$ fm, and the electronic isotope shift, Eq. 1, to obtain a precise value of the deuteron charge radius in an indirect way. The resulting value

$$r_d(\mu p + \text{iso}) = 2.12771(22)\ \text{fm} \qquad (13)$$

was given in (*9*) and is indicated as "μp+ iso" in Figs. 2 and 3. It is the most accurate value of the deuteron RMS charge radius and is independent of the TPE contribution in μd.

Using this "expected" deuteron radius from Eq. 13 in the theory expression for the LS in μd, Eq. 7, yields an experimental value for the TPE contribution to the LS in μd

$$\Delta E_{LS}^{TPE}(\text{exp}) = 1.7638(68)\,\text{meV} \qquad (14)$$

from the measured LS in Eq. 5. It is 2.6σ larger than the calculated value, Eq. 8, but three times more accurate, making it a benchmark for ab initio calculations of the deuteron (*2*, *19*, *20*, *22*) or analysis of virtual Compton scattering data (*21*).

In a similar manner, we determine the experimental value of the polarizability—i.e., the inelastic part of the TPE contribution to the 2S-HFS—using our measured HFS, Eq. 6, Eq. 42 of (*13*), and the Zemach radius of the deuteron $r_Z = 2.593(16)$fm from (*40*). We obtain

$$\Delta E_{HFS}^{pol}(\text{exp}) = 0.2178(74)\,\text{meV} \qquad (15)$$

where the experimental uncertainty is by far the dominant one. This agrees with the theoretical value $\Delta E_{HFS}^{pol}(\text{theo}) = 0.2226(49)$ meV, which has been calculated only recently (*16*).

Finally, we note that the reasoning that leads to Eq. 13 can of course be inverted. Using the measured muonic deuteron charge radius, Eq. 9, and the electronic isotope shift, Eq. 1, we obtain a new value for the proton radius

$$r_p(\mu d + \text{iso}) = 0.8356(20)\,\text{fm} \qquad (16)$$

confirming the "small" proton charge radius from muonic hydrogen (*8*, *9*), further amplifying the "proton radius puzzle" (*10*, *11*) (see Fig. 4).

Ultimately, only new experiments can shed more light on the proton and deuteron radius discrepancies. A lot of activity exists in elastic electron scattering (*41*, *42*), with the hope for refined values of r_p and r_d. Muon scattering on the proton will be able to check the BSM hypothesis (*43*). Moreover,

several atomic physics measurements are underway to verify and improve the Rydberg constant and the proton and deuteron radius from regular (electronic) hydrogen and deuterium (*44*–*46*).

REFERENCES AND NOTES

1. P. J. Mohr, B. N. Taylor, D. B. Newell, *Rev. Mod. Phys.* **84**, 1527–1605 (2012).
2. R. Machleidt, *Phys. Rev. C Nucl. Phys.* **63**, 024001 (2001).
3. H. C. Urey, F. G. Brickwedde, G. M. Murphy, *Phys. Rev.* **39**, 164–165 (1932).
4. C. G. Parthey *et al.*, *Phys. Rev. Lett.* **104**, 233001 (2010).
5. U. D. Jentschura *et al.*, *Phys. Rev. A* **83**, 042505 (2011).
6. J. C. Bernauer *et al.*, *Phys. Rev. Lett.* **105**, 242001 (2010).
7. I. Sick, D. Trautmann, *Nucl. Phys. A.* **637**, 559–575 (1998).
8. R. Pohl *et al.*, *Nature* **466**, 213–216 (2010).
9. A. Antognini *et al.*, *Science* **339**, 417–420 (2013).
10. R. Pohl, R. Gilman, G. A. Miller, K. Pachucki, *Annu. Rev. Nucl. Part. Sci.* **63**, 175–204 (2013).
11. C. E. Carlson, *Prog. Part. Nucl. Phys.* **82**, 59–77 (2015).
12. M. Diepold *et al.*, *Phys. Rev. A* **88**, 042520 (2013).
13. J. J. Krauth *et al.*, *Ann. Phys. (N.Y.)* **366**, 168–196 (2016).
14. A. A. Krutov, A. P. Martynenko, *Phys. Rev. A* **84**, 052514 (2011).
15. E. Borie, *Ann. Phys. (N.Y.)* **327**, 733–763 (2012).
16. R. N. Faustov, A. P. Martynenko, G. A. Martynenko, V. V. Sorokin, *Phys. Rev. A* **90**, 012520 (2014).
17. R. N. Faustov, A. P. Martynenko, G. A. Martynenko, V. V. Sorokin, *Phys. Rev. A* **92**, 052512 (2015).
18. K. Pachucki, *Phys. Rev. Lett.* **106**, 193007 (2011).
19. J. L. Friar, *Phys. Rev. C Nucl. Phys.* **88**, 034003 (2013).
20. O. Hernandez, C. Ji, S. Bacca, N. Nevo Dinur, N. Barnea, *Phys. Lett. B* **736**, 344–349 (2014).
21. C. E. Carlson, M. Gorchtein, M. Vanderhaeghen, *Phys. Rev. A* **89**, 022504 (2014).
22. K. Pachucki, A. Wienczek, *Phys. Rev. A* **91**, 040503 (2015).
23. A. Antognini *et al.*, *IEEE J. Quantum Electron.* **45**, 993–1005 (2009).
24. A. Antognini *et al.*, *Opt. Commun.* **253**, 362–374 (2005).
25. L. S. Rothman *et al.*, *J. Quant. Spectrosc. Radiat. Transf.* **110**, 533–572 (2009).
26. J. Vogelsang *et al.*, *Opt. Express* **22**, 13050–13062 (2014).
27. L. Ludhova *et al.*, *Nucl. Instrum. Methods Phys. Res. A* **540**, 169–179 (2005).
28. L. M. P. Fernandes *et al.*, *J. Instrum.* **2**, P08005 (2007).
29. P. Amaro *et al.*, *Phys. Rev. A* **92**, 022514 (2015).
30. A. Antognini *et al.*, *Ann. Phys. (N.Y.)* **331**, 127–145 (2013).
31. R. Pohl *et al.*, https://arxiv.org/abs/1607.03165 (2016).
32. D. Tucker-Smith, I. Yavin, *Phys. Rev. D Part. Fields Gravit. Cosmol.* **83**, 101702 (2011).
33. B. Batell, D. McKeen, M. Pospelov, *Phys. Rev. Lett.* **107**, 011803 (2011).
34. C. E. Carlson, B. C. Rislow, *Phys. Rev. D Part. Fields Gravit. Cosmol.* **86**, 035013 (2012).
35. F. Jegerlehner, A. Nyffeler, *Phys. Rep.* **477**, 1–110 (2009).
36. G. A. Miller, *Phys. Lett. B* **718**, 1078–1082 (2013).
37. U. D. Jentschura, *Phys. Rev. A* **88**, 062514 (2013).
38. G. A. Miller, *Phys. Rev. C Nucl. Phys.* **91**, 055204 (2015).
39. F. Biraben, *Eur. Phys. J. Spec. Top.* **172**, 109–119 (2009).
40. J. Friar, I. Sick, *Phys. Lett. B* **579**, 285–289 (2004).
41. A. Gasparian, *EPJ Web Confer.* **73**, 07006 (2014).
42. M. Mihovilovič, H. Merkel, A. Weber, *EPJ Web Confer.* **81**, 01009 (2014).
43. R. Gilman, *AIP Conf. Proc.* **1563**, 167–170 (2013).
44. A. Beyer *et al.*, *Ann. Phys. (Berlin)* **525**, 671–679 (2013).
45. A. C. Vutha *et al.*, *Bull. Am. Phys. Soc.* **57**, Q1.138 (2012).
46. S. Galtier *et al.*, *J. Phys. Chem. Ref. Data* **44**, 031201 (2015).
47. X. Zhan *et al.*, *Phys. Lett. B* **705**, 59–64 (2011).
48. M. A. Belushkin, H.-W. Hammer, U.-G. Meissner, *Phys. Rev. C Nucl. Phys.* **75**, 035202 (2007).
49. I. T. Lorenz, U.-G. Meissner, H.-W. Hammer, Y. B. Dong, *Phys. Rev. D Part. Fields Gravit. Cosmol.* **91**, 014023 (2015).
50. A. Antognini, https://arxiv.org/abs/1512.01765 (2015).

ACKNOWLEDGMENTS

We thank E. Borie for the calculations that made this measurement possible; I. Sick for insightful discussions; L.M. Simons and B. Leoni for setting up the cyclotron trap; R. Rosenfelder and C. Hoffman for support; H. Brückner, K. Linner, W. Simon, O. Huot and Z. Hochman for technical support; P. Maier-Komor, K. Nacke, M. Horisberger, A. Weber, L. Meier, and J. Hehner for thin foils and windows; N. Schlumpf, U. Hartmann, and M. Gaspar for electronics; S. Spielmann-Jaeggi and L. Carroll for optical measurements; Ch. Parthey and M. Herrmann for their help; Th. Udem for insightful discussions; the MEG-collaboration for a share of valuable beamtime; and A. Voss, B. Weichelt and J. Fruechtenicht for the loan of a laser pump diode. We acknowledge the essential contributions of H. Hofer and V. W. Hughes in the initial stages of the experiment and thank K. Kirch for his continuous support. We also thank the PSI accelerator division, the Hallendienst, the workshops at PSI, MPQ, and Fribourg, and other support groups for their valuable help. We acknowledge support from the European Research Council (ERC StG. 279765), the Max Planck Society and the Max Planck Foundation, the Swiss National Science Foundation (project 200020-100632, 200021L_138175, 200020_159755, 200021_165854) and the Swiss Academy of Engineering Sciences, the BQR de l'UFR de physique fondamentale et appliquée de l'Université Pierre et Marie Curie- Paris 6, the program PAI Germaine de Staël no. 07819NH du ministère des affaires étrangères France, the Fundação para a Ciência e a Tecnologia (Portugal) and FEDER (project PTDC/FIS/102110/2008 and grants SFRH/BPD/46611/2008, SFRH/BPD/74775/2010, and SFRH/BPD/76842/2011), Deutsche Forschungsgemeinschaft (DFG) GR 3172/9-1 within the D-A-CH framework, and Ministry of Science and Technology, Taiwan, no. 100-2112-M-007-006-MY3. P.I. acknowledges support by the "ExtreMe Matter Institute, Helmholtz Alliance HA216/EMMI." Reasonable requests for sharing the data should be addressed to R.P. All authors contributed substantially to this work.

13 January 2016; accepted 20 July 2016
10.1126/science.aaf2468

EXTRASOLAR PLANETS

Direct imaging discovery of a Jovian exoplanet within a triple-star system

Kevin Wagner,[1]* Dániel Apai,[1,2] Markus Kasper,[3] Kaitlin Kratter,[1] Melissa McClure,[3] Massimo Robberto,[4,5] Jean-Luc Beuzit[6,7]

Direct imaging allows for the detection and characterization of exoplanets via their thermal emission. We report the discovery via imaging of a young Jovian planet in a triple-star system and characterize its atmospheric properties through near-infrared spectroscopy. The semimajor axis of the planet is closer relative to that of its hierarchical triple-star system than for any known exoplanet within a stellar binary or triple, making HD 131399 dynamically unlike any other known system. The location of HD 131399Ab on a wide orbit in a triple system demonstrates that massive planets may be found on long and possibly unstable orbits in multistar systems. HD 131399Ab is one of the lowest mass (4 ± 1 Jupiter masses) and coldest (850 ± 50 kelvin) exoplanets to have been directly imaged.

Thousands of planets around other stars have been discovered (*1*, *2*), revealing a greater diversity than predicted by traditional planet formation models based on the solar system. Extreme examples are planets within binary and multiple-star systems, which form and evolve in variable radiation and gravitational fields. Direct imaging allows for the detection and spectroscopic characterization of long-period giant planets, thus enabling constraints to be placed on planet formation models via predictions of planet population statistics and atmospheric properties (*3*). However, most direct imaging surveys have traditionally excluded visual binary or multiple systems whose separations are less than a few hundred astronomical units (AUs). These exclusions are based on the assumption that such planetary systems would either be disrupted or never form, as well as the increased technical complexity of detecting a planet among the scattered light of multiple stars. As a result of this observational bias, most directly imaged exoplanets have been found around single stars.

Because multistar systems are as numerous as single stars (*4*), building a complete census of long-period giant planets requires investigation of both configurations. In principal, planets on wide orbits (detectable by direct imaging) might arise more frequently in multistar systems because of planet-planet or planet-star interactions (*5*, *6*). Such interactions could even produce planets on chaotic orbits that wander between the stars (*7*, *8*). To investigate the frequency of long-period giant planets both around single stars and in multistar systems, we are using the Very Large Telescope (VLT) and the Spectro-Polarimetric High-Contrast Exoplanet Research instrument [SPHERE (*9*)] to sample a population of ~100 young single and multiple A-type stars in the nearby Upper Scorpius-Centaurus-Lupus association. Here we report the discovery of the first planet detected in our ongoing survey and the widest-orbit planet within a multistar system.

Observations and discovery of HD 131399Ab

HD 131399 (also known as HIP72940) is a triple system (*10*) in the 16 ± 1–million–year–old Upper

[1]Department of Astronomy and Steward Observatory, The University of Arizona, 933 North Cherry Avenue, Tucson, AZ 85721, USA. [2]Lunar and Planetary Laboratory, The University of Arizona, 1640 East University Boulevard, Tucson, AZ 85718, USA. [3]European Southern Observatory (ESO), Karl-Schwarzschild-Strasse 2, D-85748 Garching, Germany. [4]Space Telescope Science Institute, 3700 San Martin Drive, Baltimore, MD 21218, USA. [5]Department of Physics and Astronomy, Johns Hopkins University, Baltimore, MD 21218, USA. [6]Université Grenoble Alpes, Institut de Planétologie et d'Astrophysique de Grenoble (IPAG), F-38000 Grenoble, France. [7]CNRS, IPAG, F-38000 Grenoble, France.
*Corresponding author. Email: kwagner@as.arizona.edu

Laser spectroscopy of muonic deuterium

Randolf Pohl, François Nez, Luis M. P. Fernandes, Fernando D. Amaro, François Biraben, João M. R. Cardoso, Daniel S. Covita, Andreas Dax, Satish Dhawan, Marc Diepold, Adolf Giesen, Andrea L. Gouvea, Thomas Graf, Theodor W. Hänsch, Paul Indelicato, Lucile Julien, Paul Knowles, Franz Kottmann, Eric-Olivier Le Bigot, Yi-Wei Liu, José A. M. Lopes, Livia Ludhova, Cristina M. B. Monteiro, Françoise Mulhauser, Tobias Nebel, Paul Rabinowitz, Joaquim M. F. dos Santos, Lukas A. Schaller, Karsten Schuhmann, Catherine Schwob, David Taqqu, João F. C. A. Veloso, Aldo Antognini and The CREMA Collaboration (August 11, 2016)
Science **353** (6300), 669-673. [doi: 10.1126/science.aaf2468]

Editor's Summary

The deuteron is too small, too

The radius of the proton has remained a point of debate ever since the spectroscopy of muonic hydrogen indicated a large discrepancy from the previously accepted value. Pohl *et al.* add an important clue for solving this so-called proton radius puzzle. They determined the charge radius of the deuteron, a nucleus consisting of a proton and a neutron, from the transition frequencies in muonic deuterium. Mirroring the proton radius puzzle, the radius of the deuteron was several standard deviations smaller than the value inferred from previous spectroscopic measurements of electronic deuterium. This independent discrepancy points to experimental or theoretical error or even to physics beyond the standard model.

Science, this issue p. 669

Science (print ISSN 0036-8075; online ISSN 1095-9203) is published weekly, except the last week in December, by the American Association for the Advancement of Science, 1200 New York Avenue NW, Washington, DC 20005.